Article:
Arakawa, K, Marinica, M-C, Fitzgerald, S orcid.org/0000-0003-2865-3057 et al. (15 more authors) (2020) Quantum de-trapping and transport of heavy defects in tungsten. Nature Materials, 19. pp. 508-511. ISSN 1476-1122

https://doi.org/10.1038/s41563-019-0584-0

Quantum de-trapping and transport of heavy defects in tungsten

Kazuto Arakawa[1*], Mihai-Cosmin Marinica[2], Steven Fitzgerald[3], Laurent Proville[2], Duc Nguyen-Manh[4], Sergei L. Dudarev[4], Pui-Wai Ma[4], Thomas D. Swinburne[5], Alexandra M. Goryaeva[2], Tetsuya Yamada[6], Takafumi Amino[7], Shigeo Arai[8], Yuta Yamamoto[8], Kimitaka Higuchi[8], Nobuo Tanaka[8], Hidehiro Yasuda[9], Tetsuya Yasuda[9], Hirotaro Mori[9]

[1]*Next Generation TATARA Co-Creation Centre, Organization for Industrial Innovation, Shimane University, 1060 Nishikawatsu, Matsue 690-8504, Japan.*

[2]*DEN-Service de Recherches de Métallurgie Physique, CEA, Université Paris-Saclay, F-91191, Gif-sur-Yvette, France.*

[3]*Department of Applied Mathematics, University of Leeds, Leeds LS2 9JT, UK*

[4]*CCFE, United Kingdom Atomic Energy Authority, Culham Science Centre, Oxfordshire OX14 3DB, United Kingdom.*

[5]*CINaM-Aix Marseille Université-CNRS, 13009 Marseille, France.*

[6]*Railway, Automotive & Machinery Parts Unit Osaka Steel Works, Nippon Steel & Sumitomo Metal Corporation, 1-109, Shimaya 5-chome, Konohana-ku, Osaka 554-0024, Japan.*

[7]*Advanced Technology Research Laboratories, Nippon Steel & Sumitomo Metal Corporation, 1-8 Fuso-Cho, Amagasaki, Hyogo 660-0891, Japan.*

[8]*Institute of Materials and Systems for Sustainability, Nagoya University, Nagoya 464-8603, Japan.*

[9]*Research Centre for Ultra-High Voltage Electron Microscopy, Osaka University, 7-1 Mihogaoka, Ibaraki, Osaka 567-0047, Japan.*

*email: arakawa@riko.shimane-u.ac.jp

The diffusion of defects in crystalline materials[1] controls macroscopic behaviour of a wide range of processes, including alloying, precipitation, phase transformation, and creep[2]. In real materials, intrinsic defects are unavoidably bound to static trapping centres such as impurity atoms, meaning that their diffusion is dominated by de-trapping processes. It is generally believed that de-trapping occurs only by thermal activation. Here, we report the direct observation of the quantum de-trapping of defects below around 1/3 of the Debye temperature. We successfully monitored the de-trapping and migration of self-interstitial atom clusters, strongly trapped by impurity atoms in tungsten, by triggering de-trapping out of equilibrium at cryogenic temperatures, using high-energy electron irradiation and in-situ transmission electron microscopy. The quantum-assisted de-trapping leads to low-temperature diffusion rates orders of magnitude higher than a naive classical estimate suggests. Our analysis shows that this phenomenon is generic to any crystalline material.

Under high-energy irradiation (or extreme mechanical deformation), atoms in a crystal can be displaced significantly from their lattice positions, forming vacancy and self-interstitial atom (SIA) defects. These are ultimately responsible for severe degradation of the mechanical properties of materials, such as hardening, swelling, and embrittlement[3]. Understanding the basic mechanisms controlling the formation and diffusion of defects[4-6] is critical for the development of future next-generation energy systems.

In the field of material science, to the best of our knowledge, all the observed migration processes of species heavier than H or He[7,8] have been interpreted as

resulting from thermal activation characterized by the Arrhenius rate[9], or phonon dragging[10,11]. No apparent quantum effects have been detected[12], although they have been theoretically considered for SIAs[13-15] and screw dislocations[16]. Quantum effects have also been observed on metal surfaces[17]. We focus here on the low temperature diffusion of SIA clusters in tungsten as a model for crystal defects in heavy-atom systems.

The lowest-energy SIA configuration in tungsten (and other non-magnetic body-centred-cubic (bcc) transition metals) is a ⟨111⟩ crowdion, in which atomic displacements are confined almost entirely to a ⟨111⟩ string containing an extra atom. The defect is delocalized: it involves many more than one atom, as the displacement field is spread down the string, resulting in very low barriers to translation (known as *Peierls* barriers, see Supplementary Discussion 1a and Fig. ED1). Hence crowdions perform one-dimensional (1D) diffusion along their axis with a low (meV scale) activation energy[10,18,19]. Similarly to single crowdions, SIA clusters in the form of **b** = ½⟨111⟩ dislocation loops undergo 1D glide diffusion in the direction of the Burgers' vector **b**. This phenomenon has been studied using classical molecular dynamics simulations (MD)[20-24] and transmission electron microscopy (TEM)[5,25] for α-iron and other metals and alloys.

According to MD studies, the activation energy (Peierls barrier) for cluster diffusion is less than 0.1 eV[20,22], meaning they are thermally mobile even at very low temperatures. In any real material however, impurity atoms (mainly carbon and nitrogen) act as traps by binding to the clusters. Vacancies (expected at high density under irradiation) will mutually annihilate with SIAs at the cluster boundary.

Previous studies, using resistivity recovery and internal friction experiments[9], have shown that low-temperature cluster migration in tungsten (and other bcc metals) is strongly influenced by the concentration of impurity atoms[26-28].

These traps are deep enough (~1 eV, see Supplementary Discussion 1b and Fig. ED2) to prevent TEM observation of the clusters' thermal escape and subsequent motion on experimental timescales, even at 300 K, and they remain immobile. To overcome this, we used the electron beam in transmission electron microscopes such as a high-voltage electron microscope (HVEM) to enhance the vacancy mobility and reduce the effective trap depth. In the absence of the electron beam, vacancies are immobile up to 620-900K[9], but in our experiment, the momentum imparted by the incident electrons moves the vacancies up to 100 times per second. The experimental system is shown schematically in Fig. 1, and operates as follows.

First, a high energy (2000 keV) electron beam is used to create displacement damage, vacancies and SIAs at 105 K, before aging at 300 K. This allows the SIA clusters to nucleate and grow to nanoscale, with impurities bound to their perimeters (where the binding energy is greatest). At these temperatures, the vacancies are thermally immobile and remain dispersed throughout the sample. A lower energy (100-1000 keV) electron beam is then turned on to illuminate the sample. The energy of incident electrons is too low to create additional vacancies and SIAs, but high enough to athermally move the existing vacancies (see Methods). Under the beam, the previously trapped clusters begin to move (Fig. 1; Supplementary Video 1). The principal quantity we monitor is the cluster motion frequency. The precise definition

of this quantity, together with its dependence on the experimental irradiation conditions, is given in Methods and illustrated in Fig. 2. Perhaps the most striking feature of our study is the possibility to resolve the SIA clusters' thermal and quantum-mechanical motion, even in the presence of a flux of vacancies. In Methods we describe in detail how this is achieved.

The key features of the observed motion of SIA clusters are as follows: Firstly, hops are rare events, i.e. the clusters spend far more time being trapped than travelling between traps. Secondary, clusters sometimes move back and forth between fixed points in the sample. Thirdly, clusters are observed to shrink under the beam. Fourthly, motion frequency depends strongly on temperature. The first and second key features tell us that the clusters are escaping from the impurity traps, moving quickly through the lattice before being subsequently trapped again. The third key feature tells us how this occurs: the radiation-mobilized vacancies move through the crystal, attracted to the areas of highly compressive strain at the cluster boundaries. Here they annihilate with the SIAs at the cluster boundaries, reducing the size of the cluster, and increasing the separation between the impurity atom and the cluster boundary. The impurity-cluster interaction is strong but short-ranged (see Supplementary Discussion 1b and Fig. ED2), and rapidly vanishes over only a few lattice spacings, so that the traps are now much shallower, and making cluster escape easier (Fig. 2abc). We now turn to the fourth key feature, the temperature dependence, which demonstrates that the low temperature escapes are quantum mechanical in nature. It is noted that, for this purpose, we set the experimental system so that the cluster escape processes by the direct electron collision with a cluster itself[29] or the impurity that traps the cluster[30] can be neglected (Methods).

Figure 3 is an Arrhenius plot showing the logarithm of the motion frequency vs. inverse temperature. Hops due to thermal escape from potential wells of depth $\Delta V \gg k_B T$ have a characteristic rate $\propto \exp(-\Delta V/k_B T)$, corresponding to a straight line on an Arrhenius plot. This appears to be the case at higher temperatures $T \geq 50$ K and the slope suggests that ΔV is higher than 10 meV. As temperature is reduced, 17 K $\leq T \leq$ 50 K, the slope flattens as the de-trapping mechanism changes from classical thermal escape to temperature-independent quantum mechanical diffusion.

The measured rates result from three independent processes: the athermal radiation-driven vacancy migration under the beam (rate Γ_{vac}), the fluctuation-driven escape of the cluster from the trap (depth ΔV_{trap}, rate Γ_{trap}), and finally the traversal of the Peierls barrier intrinsic to the crystal (depth ΔV_P, rate Γ_P) (see Methods).

Figure 3a shows attempted classical fits for all barriers $10\text{meV} \leq \Delta V = \Delta V_P + \Delta V_{trap} \leq 90\text{meV}$. Note that the Peierls traversal rate is non-Arrhenius (since ΔV_P is not more than $k_B T$, see Methods), but no possible classical form for the rate can explain the observed values. (We are able to state with confidence that the sample temperatures continue to decrease below 50 K, and are not significantly affected by beam heating – see Supplementary Discussion 2 and Fig. ED3).

In Fig. 3b, we use a quantum mechanical form for the escape rate Γ^{QM}, derived from the quantized nature of the crystal phonons (see Methods). These obey the Bose-Einstein rather than the Boltzmann statistics, and their zero-point fluctuations increase the average energy available for the cluster to overcome the barrier, thus increasing

151 the low temperature rates, in excellent agreement with experimental observations.
152 Moreover, the same quantum rates simultaneously fit two independent datasets,
153 acquired at two different electron accelerating voltages. This proves that the same
154 fundamentally quantum mechanism explains both datasets.
155
156 We are able to obtain acceptable fits for all barriers between 10 and 90 meV. To
157 narrow this down, we consider the critical temperature τ_c below which classical
158 physics breaks down (see Methods). This depends on the barrier height: Figure 2
159 shows that the 90 meV fit clearly failing below 140 K, whereas the 10 meV one
160 appears reasonable down to around 50 K. τ_c depends on the phonon density of states,
161 and is estimated[31] to be 101 K for pure tungsten (about 1/3 of the Debye temperature).
162 Fitted values for τ_c are also shown in Fig. 3, and the value of 101 K is consistent with
163 a barrier height of 30 – 44 meV. We note that the resistivity recovery and internal
164 friction experiments correspond to the barrier height of 15 – 60 meV[9,26-28].
165
166 Other manifestations of quantum behaviour are in principle possible, in particular the
167 deep tunneling of the entire cluster. However, fitting the data to this functional form
168 requires unrealistic values for the cluster's effective mass (see Methods), and we
169 conclude that, over the range of temperatures probed by our experiments, quantized
170 phonons facilitating the clusters' escape from traps that are 30 – 44 meV deep provide
171 the optimal explanation of the data.
172
173
174 In this study we have performed the direct investigation of cryogenic defect diffusion
175 using in-situ TEM. Our unique experimental system allowed us to manipulate the

effective potential wells encountered by SIA clusters, reducing their depth until we could probe the quantum mechanical nature of their de-trapping. The quantum transport becomes dominant below around 1/3 of the Debye temperature. Moreover, the observed behaviour derives from quantized phonons, which drive the stochastic fluctuations of objects that are themselves too heavy to tunnel significantly. This likely affects the low temperature transport of defects in many crystalline materials. Our results also demonstrate the importance of quantum effects for low temperature defect evolution even in heavy atom systems.

References

1 Mehrer, H. *Diffusion in Solids*. Vol. 155 (Springer, 2007).

2 Gupta, D. *Diffusion Processes in Advanced Technological Materials*. (William Andrew Inc., 2005).

3 Gary, S. W. *Fundamentals of Radiation Materials Science*. (Springer, 2007).

4 Fu, C.-C., Torre, J. D., Willaime, F., Bocquet, J.-L. & Barbu, A. Multiscale modelling of defect kinetics in irradiated iron. *Nature Materials* **4**, 68-74 (2005).

5 Arakawa, K. *et al.* Observation of the one-dimensional diffusion of nanometer-sized dislocation loops. *Science* **318**, 956-959, doi:10.1126/science.1145386 (2007).

6 Bai, X.-M., Voter, A. F., Hoagland, R. G., Nastasi, M. & Uberuaga, B. P. Efficient Annealing of Radiation Damage Near Grain Boundaries via Interstitial Emission. *Science* **327**, 1631-1634, doi:10.1126/science.1183723 (2010).

7 Kadono, R. *et al.* Quantum diffusion of positive muons in copper. *Physical Review B* **39**, 23-41 (1989).

8 Sundell, P. G. & Wahnström, G. Activation energies for quantum diffusion of hydrogen in metals and on metal surfaces using delocalized nuclei within the density-functional theory. *Physical Review Letters* **92**, 155901 (2004).

9 Ehrhart, P., Jung, P., Schultz, H. & Ullmaier, H. *Atomic Defects in Metals*. Vol. 25 (Springer-Verlag, Berlin, 1991).

10 Derlet, P. M., Nguyen-Manh, D. & Dudarev, S. L. Multiscale modeling of crowdion and vacancy defects in body-centered-cubic transition metals. *Physical Review B* **76**, 054107 (2007).

11 Swinburne, T. D., Dudarev, S. L. & Sutton, A. P. Classical Mobility of Highly Mobile Crystal Defects. *Physical Review Letters* **113**, 215501 (2014).

12 Wollenberger, H. J. in *Physical Metallurgy, Part II* (eds R. W. Chan & P. Haasen) 1139 (North Holland Physics Publishing, Amsterdam, 1983).

13 Pushkarov, D. I. Quantum theory of crowdions at low temperatures. *Soviet Journal of Experimental and Theoretical Physics* **37** (1973).

14 Flynn, C. P. Resonance mode hopping and the stage I annealing of metals. *Thin Solid Films* **25**, 37-43, doi:http://dx.doi.org/10.1016/0040-6090(75)90242-4 (1975).

15 Swinburne, T. D., Ma, P.-W. & Dudarev, S. L. Low temperature diffusivity of self-interstitial defects in tungsten. *New Journal of Physics* **19**, 073024 (2017).

16 Proville, L., Rodney, D. & Marinica, M.-C. Quantum effect on thermally activated glide of dislocations. *Nat Mater* **11**, 845-849, doi:http://www.nature.com/nmat/journal/v11/n10/abs/nmat3401.html#supplementary-information (2012).

17 Ohresser, P. *et al.* Surface Diffusion of Cr Adatoms on Au(111) by Quantum Tunneling. *Physical Review Letters* **95**, 195901 (2005).

18 Fitzgerald, S. P. & Nguyen-Manh, D. Peierls potential for crowdions in the bcc transition metals. *Physical Review Letters* **101**, 115504 (2008).

19 Amino, T., Arakawa, K. & Mori, H. Detection of one-dimensional migration of single self-interstitial atoms in tungsten using high-voltage electron microscopy. *Sci Rep* **6**, 26099, doi:10.1038/srep26099 (2016).

20 Wirth, B. D., Odette, G. R., Maroudas, D. & Lucas, G. E. Dislocation loop structure, energy and mobility of self-interstitial atom clusters in bcc iron. *J Nucl Mater* **276**, 33-40, doi:http://dx.doi.org/10.1016/S0022-3115(99)00166-X (2000).
21 Marian, J. *et al.* Dynamics of self-interstitial cluster migration in pure α-Fe and Fe-Cu alloys. *Physical Review B* **65**, 144102 (2002).
22 Osetsky, Y. N., Bacon, D. J., Serra, A., Singh, B. N. & Golubov, S. I. One-dimensional atomic transport by clusters of self-interstitial atoms in iron and copper. *Philos Mag* **83**, 61-91, doi:10.1080/0141861021000016793 (2003).
23 Dudarev, S. L. The non-Arrhenius migration of interstitial defects in bcc transition metals. *Comptes Rendus Physique* **9**, 409-417, doi:10.1016/j.crhy.2007.09.019 (2008).
24 Swinburne, T. D., Dudarev, S. L., Fitzgerald, S. P., Gilbert, M. R. & Sutton, A. P. Theory and simulation of the diffusion of kinks on dislocations in bcc metals. *Physical Review B* **87**, 064108 (2013).
25 Arakawa, K., Amino, T. & Mori, H. One-dimensional glide motion of "naked" 1/2<111> prismatic dislocation loops in iron. *ISIJ International* **54**, 2421-2424 (2014).
26 Dausinger, F. & Schultz, H. Long-range migration of self-interstitial atoms in tungsten. *Physical Review Letters* **35**, 1773-1775 (1975).
27 Dausinger, V. F. Die Tieftemperaturerholung in elektronenbestrahltem Wolfram. *Philosophical Magazine A* **37**, 819-836, doi:10.1080/01418617808239211 (1978).
28 Mizubayashi, H. & Okuda, S. Elastic after-effect studies of self-interstitials in tungsten after fast neutron irradiation at 5 K. *Radiation Effects* **54**, 201-215, doi:10.1080/00337578108210049 (1981).
29 Dudarev, S. L., Derlet, P. M. & Woo, C. H. Driven mobility of self-interstitial defects under electron irradiation. *Nuclear Instruments and Methods in Physics Research Section B: Beam Interactions with Materials and Atoms* **256**, 253-259, doi:10.1016/j.nimb.2006.12.013 (2007).
30 Satoh, Y., Matsui, H. & Hamaoka, T. Effects of impurities on one-dimensional migration of interstitial clusters in iron under electron irradiation. *Physical Review B* **77**, 94135, doi:10.1103/PhysRevB.77.094135 (2008).
31 Ashcroft, N. W. & Mermin, N. D. *Solid State Physics*. (College Edition, New York, 1978).

Acknowledgements

This work was financially supported by JSPS KAKENHI (Grant No. 15H04244, and 18K18951), ImPACT Program of Council for Science, Technology and Innovation (Cabinet Office, Government of Japan), Q-LEAP Program (MEXT: Ministry of Education, Culture, Sports, Science and Technology - Japan), and the Iron and Steel Institute of Japan Research Promotion Grant. Part of this work was supported by the "Advanced Characterization Nanotechnology Platform, Nanotechnology Platform Programs" of MEXT, at Institute of Materials and Systems for Sustainability (Nanotechnology Open Facilities) in Nagoya University and at Research Centre for Ultra-High Voltage Electron Microscopy (Nanotechnology Open Facilities) in Osaka University, and TATARA Nanotechnology Project Centre

in Shimane University. M.C.M., L.P. and A.M.G. acknowledges support from the GENCI - (CINES/CCRT) computer centre under Grant No. A0070906973. A.M.G. and M.C.M acknowledges the financial support of the Cross-Disciplinary Program on Numerical Simulation of CEA, the French Alternative Energies and Atomic Energy Commission. S.P.F. acknowledges support from the UK EPSRC, grant number EP/R005974/1. The work at CCFE has been carried out within the framework of the EUROfusion Consortium and has received funding from the Euratom research and training programme 2019-2020 under grant agreement No 633053 and funding from the RCUK Energy Programme [grant number EP/P012450/1]. The views and opinions expressed herein do not necessarily reflect those of the European Commission.

Author contributions

K.A., M.C.M. and L.P. designed the study. K.A., T.Y., T.A., S.A., Y.Y., K.H., N.T., H.Y., T.Y. and H.M. performed the experiments. M.C.M., S.P.F., L.P., D.N.M., A.M.G., S.L.D., P.W.M. and T.D.S. performed the theoretical works. K.A., M.C.M., S.P.F., and S.L.D. wrote the main draft. All authors discussed the results and commented on the manuscript.

Additional information

Supplementary information is available in the online version of the paper. Reprints and permissions information is available online at www.nature.com/reprints. Correspondence and requests for materials should be addressed to K.A.

Competing financial interests

The authors declare no competing financial interest.

METHODS

Specimen preparation. We cut (011) discs from one grain of an ingot of high-purity coarse-grained polycrystalline tungsten (99.9999 mass % JX Nippon Mining & Metals Co., Tokyo, Japan; impurity amounts of the ingot are given in Ref. [32]). The discs were thinned to 0.1mm, using spark erosion and mechanical polishing, then perforated at the centre by electropolishing so the periphery of the hole became cross-sectionally wedge-shaped for TEM observations.

Production of SIA clusters. We used high-energy electron irradiation in a HVEM (Hitachi H-3000) to create SIAs and vacancies in the thin foil specimens. The acceleration voltage was 2000 kV, and a temperature of 105 K was maintained using a liquid-nitrogen-cooled specimen holder (Oxford Instruments). We note that the thermal migration of vacancies is frozen at temperatures below 620-900 K[9]. The beam flux was 1×10^{24} $m^{-2}s^{-1}$, and the dose was 4×10^{25} m^{-2}.

During 2000-keV electron irradiation, pairs of SIAs and vacancies are produced[33] via knock-on displacement. Based on our recent work[19,32], the point defect reactions proceed as follows: most of the highly mobile 1D-moving SIAs react with vacancies, or escape to the foil surface, where they are annihilated. Surviving SIAs bind to impurity atoms and form embryonic SIA clusters, that grow by absorbing other SIAs, and take the form of $\mathbf{b} = \frac{1}{2}\langle 111 \rangle$ dislocation loops. These clusters are intrinsically highly mobile, yet they are trapped by impurities and remain stationary. Vacancies that do not react with SIAs accumulate throughout the irradiated area of the specimen.

Using TEM, the average size and density of the SIA formed clusters under the above condition were found to be approximately 3-4 nm and 4×10^{22} m^{-3}, respectively. Accumulated vacancies are not visible in the TEM. After the irradiation, the specimen was aged at approximately 300 K. This allows the clusters trapped by weak impurity atoms with shallow potential wells to thermally escape and move, leading to coalescence with other clusters[34], escape to the specimen surfaces, or to trapping by stronger impurities with deeper wells. However, even after aging for several months, we did not see any significant change in the cluster density, demonstrating that thermal escape of SIA clusters from the deeper wells hardly occurs even at 300 K.

TEM observation of the 1D motion of SIA clusters in response to high-energy

electron irradiation. We then used the electron beam to induce the vacancy mobility, with acceleration voltages of 100, 150, 300, 500 (Hitachi H-9000UHV), 1000, and 2000kV (H-3000) – all except 2000kV are below the threshold for point defect generation in tungsten[33]. Additional very intense irradiations were carried out at 1000kV using a JEOL JEM 1000K RS. Beam fluxes ranged from 5×10^{22} to 2×10^{25} $m^{-2}s^{-1}$, and temperatures ranged from 17-300 K (where no thermal migration of vacancies takes place[9]). We achieved these temperatures using liquid-helium-cooled specimen holders (Oxford Instruments), in which the temperature is measured with a thermocouple attached to the specimen mount, so the measured temperature is the average over the whole specimen.

The specimen thickness ranged from 50 to 70 nm (measured using equal-thickness fringes[35]). The observations were carried out using the weak-beam dark-field technique[36] with a reflection of $\mathbf{g} = 200$. Under this condition, all SIA clusters in the form of prismatic dislocation loops with a $\mathbf{b} = ½\langle 111 \rangle$ type Burgers vector and a diameter greater than approximately 2 nm were imaged. The dynamic response of the clusters was monitored and recorded with CCDs having frame rates of 30 fps for H-9000UHV and H-3000, and 15 fps for JEM 1000K RS.

We define the motion frequency of the clusters as the ratio of the number of cluster hops observed per unit time divided by the number of observable clusters, i.e. the average motion frequency of individual SIA clusters.

Motion frequency and the ballistic and kinetic rates of SIA clusters. Our experiments measure the average motion frequency of SIA clusters under electron irradiation as simultaneously observed in the transmission electron microscopes. The average motion frequency at irradiation (observation) time t is defined as $\nu_{\mathrm{MF}}(t) = n_{\mathrm{m}}/(n\,\Delta t)$: the ratio of the number of clusters that move (n_{m}) divided by the total number of observed clusters (n) in the observation duration Δt.

The measured rates ν_{MF} are the combined results of motion induced by directly by the irradiation, and stochastic motion induced by the underlying phonon bath. Consequently, the motion frequency is impacted by irradiation conditions, in particular the electron beam flux Φ and energy E. The temperature T also influences the experimental observations through the phonon bath, meaning that the motion frequency is a function defined on a 4 dimensional space $\nu_{\mathrm{MF}}(t, T, \Phi, E)$. Figure 3 illustrates the temperature dependence, and Fig. 2d-g shows the behaviour of the

motion frequency with respect to the other variables. Here we derive an expression for the motion frequency in the context of the experiments.

Detailed experimental analysis suggests that the shrinkage of the clusters (Fig. 2a) originates from irradiation-induced vacancy motion (Fig. 2b). Since the impurities are immobile, the erosion of the clusters by the vacancies increases the distance between them and the impurities, which leads to the de-trapping of the clusters from the impurities. We call this mechanism of the cluster de-trapping by this process the *indirect de-trapping mechanism.* Since it depends on the radiation-mobilized vacancies eroding the SIA clusters, the cluster motion frequency is proportional to the vacancy concentration, c_{V}. These vacancies are absorbed by the clusters, and other sinks such as the specimen surface, at a rate proportional to the concentration of vacancies itself: $\dot{c}_{\mathrm{V}} \propto -c_{\mathrm{V}}$. As long as no new Frenkel pairs are created, this leads to an exponential decay of vacancy concentration as a function of time, and the corresponding variation of the cluster motion frequency. This is precisely what we find in Fig. 2cd, in the limit of short observation time.

In the indirect mechanism, cluster de-trapping is also impacted by the thermal rate at which the clusters escape from the impurities. At a given cluster-impurity separation, d_k, sufficiently large that the trapping energy is low, the thermal escape rate Γ_{th}^{k} is governed by the cluster-impurity trapping energy $\Delta V_{\mathrm{trap}}^{k}$ for that distance (see next section). If we have n_k cluster-impurity sets at given cluster-impurity separation d_k, then the number of clusters that jump within the observation time is $a\, c_{\mathrm{V}} n_k \Gamma_{\mathrm{th}}^{k} \Delta t$. Prefactor *a* accounts for the effect of the beam flux and energy on the observations.

Since the incident electron energy is high, what we call the *direct de-trapping mechanism* – direct collision of the electron with a cluster itself[29] or the impurity that traps the cluster[30]– can also release the cluster. The de-trapping rate Γ_{d} associated with this direct mechanism is independent of temperature and uniform in time, depending only on the concentration of cluster-trapping impurities and the flux and energy of the electrons. The probability of releasing a cluster from an impurity via the direct mechanism is $n\Gamma_{\mathrm{d}}\Delta t$.

Consequently, the measured motion frequency can be written as

$$\nu_{\mathrm{MF}} = \frac{n_{\mathrm{indirect}} + n_{\mathrm{direct}}}{n\,\Delta t} = \frac{\sum_k a c_{\mathrm{V}} n_k\, \Gamma_{\mathrm{th}}^{k}(T)\Delta t + n\Gamma_{\mathrm{d}}\Delta t}{n\Delta t}$$

Or, in a simpler form, if we assume that in the system the initial vacancy density $c_{\mathrm{V}}(0)$ decreases in time with a decay factor α_{v} :

$$\nu_{\mathrm{MF}} \sim \sum_k a\, c_{\mathrm{V}}(0) e^{-\alpha_{\mathrm{v}} t} \frac{\Gamma_{\mathrm{th}}^k(T) n_k}{n} + \Gamma_{\mathrm{d}} = e^{-\alpha_{\mathrm{v}} t} \left[\sum_k a\, c_{\mathrm{V}}(0) \frac{\Gamma_{\mathrm{th}}^k(T) n_k}{n} \right] + \Gamma_{\mathrm{d}}$$

This theoretical expression for the motion frequency is fully compatible with all the experimental evidence described in the body of the paper and illustrated in Fig. 2.

Firstly, the experimental observations shown in Fig. 2de indicate that the motion frequency decreases exponentially in time, and after several hundred seconds, the frequency's exponential decay becomes a constant plateau. This reflects the local exhaustion of vacancies near the clusters, and the transition to de-trapping by direct electron impacts, through what we term the direct mechanism. The $t \to \infty$ limit corresponds to the frequency of de-trapping events associated with the direct mechanism $\nu_{\mathrm{MF}} \to \Gamma_{\mathrm{d}}$. On the other hand, in the limit of $t \to 0$:

$$\nu_{\mathrm{MF}}(t \to 0) = \left[\sum_k a_k c_v(0) \frac{\Gamma_{\mathrm{th}}^k(T) n_k}{n} \right] + \Gamma_{\mathrm{d}} \sim \text{const} \times \Gamma_{\mathrm{th}}^0(T) + \Gamma_{\mathrm{d}},$$

we have access, up to multiplicative (const) and additive (Γ_{d}) constants, to the dominant thermal/quantum rate $\Gamma_{\mathrm{th}}^0(T)$ on the nature of which, classical or quantum, our study is focused. We note that the higher the beam energy, the greater is the part played by the direct mechanism of de-trapping, and the sooner the hopping rate reaches the asymptotic value. The plateaus are also higher for higher beam energies, reflecting the direct mechanism's expected variation as a function of the incident electron beam energy.

Secondly, Fig. 2f shows the cluster motion frequency's strong dependence on the beam intensity at 300 kV, clearly illustrating a role the irradiation contributes through the multiplicative constants. Note that no further Frenkel pairs are created if the beam energy is at or below 1000 kV.

Finally, Fig. 2g shows the electron energy dependence of $\nu_{\mathrm{MF}}(t \to 0,\ E)$, together with the athermal radiation-driven vacancy migration rate under the beam Γ_{vac}. The Γ_{vac} value is proportional to the product of beam flux and the cross section for radiation induced vacancy migration[37],

$$\sigma_{\mathrm{mig}} \approx \int_{E_{\mathrm{mig}}^V}^{E_{\mathrm{K,max}}} \frac{E_{\mathrm{K}}}{E_{\mathrm{mig}}^V} \frac{\mathrm{d}\sigma}{\mathrm{d}E_{\mathrm{K}}} \mathrm{d}E_{\mathrm{K}},$$

where E_{K} is the kinetic energy transferred from an incident electron to a tungsten atom neighbouring a vacancy, E_{mig}^V is the vacancy migration energy (1.78 eV[38]), and $\mathrm{d}\sigma$ is the differential cross section for the electron-tungsten atom collision calculated

using the McKinley-Feshbach formula[39]. The high degree of correlation between the two is abundantly clear, providing a further confirmation of the vacancy origin of the indirect mechanism of cluster de-trapping and migration.

A natural question is whether this approach has sufficient accuracy to reveal the classical or quantum nature of the cluster migration rate. The quantity of interest is the logarithm of the motion frequency, which can be written as:

$$\ln \nu_{\mathrm{MF}}(t \to 0) = \ln\left[\Gamma_{\mathrm{th}}^{0}(T) + \Gamma_{\mathrm{d}}\right] \sim \ln \Gamma_{\mathrm{th}}^{0}(T) + \frac{\Gamma_{\mathrm{d}}}{\Gamma_{\mathrm{th}}^{0}(T)}$$

The second term of the right side is easily estimated from the ratio of asymptotic limits $\nu_{\mathrm{MF}}(t \to 0)/\nu_{\mathrm{MF}}(t \to \infty)$. This quantity is in the order of 10^{-1} and 10^{-2} at 1000 keV and 500 keV, respectively, for 289-298 K (Fig. 2d). Also, it is shown to be no higher than 0.2 at 300 keV even at 31 K (Fig. ED4). This analysis shows that in terms of observed logarithm of $\nu_{\mathrm{MF}}(t \to 0)$, the effect of direct de-trapping mechanism is visible at the level after the first or even the second place after the decimal point. Hence, the direct and indirect contributions to the motion frequency can be reliably separated.

We provide the details of the statistical procedure used for measuring ν_{MF}. One specimen involved 1×10^2 areas for 2000-keV electron irradiation for the SIA cluster production, at maximum. The n value within one area of interest (AOI) centred at a 2000-keV electron irradiated area was $(1 - 2) \times 10^2$ for $t = 0$ s. This n value was the practical upper limit under the lowest TEM magnification enabling the observation of the cluster motion. In the time dependence of $\nu_{\mathrm{MF}}(t)$ (Figs. 2de and ED4), matching symbols correspond to the same AOI, and in the beam flux dependence of $\nu_{\mathrm{MF}}(t \to 0, \Phi)$ (Fig. 2f), energy dependence of $\nu_{\mathrm{MF}}(t \to 0, E)$ (Fig. 2g), and temperature dependence of $\nu_{\mathrm{MF}}(t \to 0, T)$ (Fig. 3), individual data points correspond to different AOIs. The error in the ν_{MF} value was evaluated under the assumption that both the distributions of n and n_{m} for a given AOI independently obey the Poisson statistics. Then, the error in a measured ν_{MF} value becomes $\nu_{\mathrm{MF}}\sqrt{\frac{1}{n} + \frac{1}{n_{\mathrm{m}}}}$. The data sets for temperature dependence of $\nu_{\mathrm{MF}}(t \to 0, T)$ under the fixed other conditions (Fig. 3) were acquired from the areas belonging to an identical TEM specimen so that the impurity concentration in the measured areas was very similar level.

Diffusion rates in quantum and classical phonon baths. The archetypal problem of a particle traversing a potential barrier has been treated exhaustively; see Ref. [40] for a thorough review. For a barrier height $\Delta V \gg k_B T$, the classical escape rate is given by the Arrhenius function $\Gamma_{th}^{cl} = f_{cl}\exp(-\Delta V/k_B T)$, where the classical prefactor f_{cl} can be loosely interpreted as an attempt frequency. As $k_B T$ rises towards ΔV the Arrhenius function breaks down, and the rate transitions to a form linear in the temperature[11,23] (manifested as a sharp steepening on an Arrhenius plot). For barriers $\Delta V \sim k_B T$ or less, the particle migrates stochastically, being slowed only by the dissipative coupling between the particle and the underlying phonon bath. This is quantified by the friction parameter γ, and the rate is proportional to $k_B T/\gamma$ [11,23,41]. If $\Delta V \ll k_B T$, the friction can be absorbed into f_{cl}[40,42]. Both standard rate formulae originate from the classical Boltzmann distribution for the phonons. For clusters escaping from traps, the barrier to be overcome is $\Delta V = \Delta V_P + \Delta V_{trap}$, the sum of the Peierls barrier and the critical binding energy of the impurity or vacancy respectively. Therefore the diffusion rate is the product of two independent probabilities: the probability related to the free migration of the SIA cluster through the Peierls potential in the absence of a trap, and the escape probability from the trap itself: $\Gamma_{th}^{cl}(T) = \Gamma_P(T) \times \Gamma_{trap}(T)$. $\Delta V_{trap} \gg k_B T$, so Γ_{trap} is Arrhenius in the classical limit. Since the Peierls barrier ΔV_P for SIA clusters (a.k.a. ½⟨111⟩ loops) is small, i.e. of order $k_B T$, the total classical rate becomes:

$$\Gamma_{th}^{cl}(T) = \text{const.} \times k_B T \times \exp\left(-\frac{\Delta V_{trap}}{k_B T}\right) \qquad (1)$$

We note that the constant prefactor above can take on a weak temperature dependence in other formulations of the rate; we obtain similar fits in either case and our conclusions are unaffected.

The full quantum-mechanical development is more complicated. Here, the Boltzmann distribution is replaced by either the Bose-Einstein (BE) or Fermi-Dirac distribution, for bosons or fermions respectively. For tungsten or impurity atoms the ground state has integer spin and hence obeys Bose-Einstein statistic. A simple way to recover the BE phonon distribution whilst retaining the form of the classical rate formulae is to renormalize the temperature to mimic the true quantum statistics[15,42,43]. Consider a crystal with periodic boundary conditions represented by *N* atoms in a box. Imposing equality of the classical and quantum energies, the (renormalized, effective) classical temperature and the (true) quantum temperature should be related by the relation:

$$(3N-3)k_B T_c = \int \mathrm{d}\omega\, \hbar\omega \left(\rho_{BE}(\omega, T_q) + \frac{1}{2}\right) n(\omega)$$

where T_c and T_q are the (renormalized, effective) classical and (true) quantum temperatures respectively. $n(\omega)$ is the density of states of the phonon gas, normalized to the number of modes, and $\rho_{BE}(\omega, T)$ is the BE distribution function. Therefore, the effective classical temperature is a function of the true quantum temperature $T_\mathrm{c} = f(T_\mathrm{q})$.

For temperatures higher than the Debye temperature T_D, $\hbar\omega \ll k_B T$, the energy of one oscillator becomes:

$$\hbar\omega\left(\rho_{\mathrm{BE}}(\omega, T_\mathrm{q}) + \frac{1}{2}\right) \approx \frac{\hbar\omega}{2} + k_\mathrm{B}T_q\left(1 - \frac{\hbar\omega}{2k_\mathrm{B}T_\mathrm{q}} + K\right) = k_\mathrm{B}T_\mathrm{q},$$

and the classical and quantum temperatures are very close. When the (true) quantum temperature T_q tends to zero K, the effective classical temperature T_c tends to a finite limit, capturing the zero point energy:

$$(3N-3)k_\mathrm{B}T_\mathrm{c} = \int \mathrm{d}\omega\ \frac{1}{2}\hbar\omega\, n(\omega)$$

The simple form $T_c = \sqrt{\tau_\mathrm{c}^2 + T_\mathrm{q}^2}$ satisfies these limits (see Fig. ED5). Therefore, the quantum rates can be estimated by simply renormalizing the temperature in equation (1) yielding:

$$\Gamma_\mathrm{th}^\mathrm{QM}(T) = \text{const.} \times k_\mathrm{B}\sqrt{\tau_\mathrm{c}^2 + T^2} \times \exp\left(-\frac{\Delta V_\mathrm{trap}}{k_\mathrm{B}\sqrt{\tau_\mathrm{c}^2 + T^2}}\right) \qquad (2)$$

We also attempted to fit the data with up to three distinct classical barrier escape mechanisms operating simultaneously. Only the quantum rates explain the observed temperature dependence.

Quantum TST rates. For deep tunneling, we computed the rate by numerically integrating the quantum transition state theory rate expression[42]

$$\Gamma_\mathrm{th}^\mathrm{QTST} = (hZ_0)^{-1}\int W(E)\mathrm{e}^{-E/k_\mathrm{B}T}\mathrm{d}E,$$

where *h* is the Planck constant and *W(E)* is the transfer integral at energy *E* for the sech-squared impurity interaction potential predicted by the Frenkel Kontorova model, (see Supplementary Discussion 1). The data can be fitted with a barrier height of 55 meV, but requires an unrealistically low effective cluster mass of $m_\mathrm{W}/200$ (m_W is the mass of one tungsten atom). The remaining parameters (potential width and curvature) are fixed by the Arrhenius limit, which applies to the highest temperature

512 points in the dataset.

513

514 **Data availability**

515 The data generated and/or analysed within the current study will be made available
516 upon reasonable request to the corresponding author.

517

518 **References**

519 32 Amino, T., Arakawa, K. & Mori, H. Activation energy for long-range
520 migration of self-interstitial atoms in tungsten obtained by direct measurement
521 of radiation-induced point-defect clusters. *Philosophical Magazine Letters* **91**,
522 86-96, doi:10.1080/09500839.2010.533133 (2011).
523 33 Maury, F., Biget, M., Vajda, P., Lucasson, A. & Lucasson, P. Frenkel pair
524 creation and stage I recovery in W crystals irradiated near threshold. *Radiation
525 Effects* **38**, 53-65, doi:10.1080/00337577808233209 (1978).
526 34 Arakawa, K., Amino, T. & Mori, H. Direct observation of the coalescence
527 process between nanoscale dislocation loops with different Burgers vectors.
528 *Acta Mater* **59**, 141-145, doi:10.1016/j.actamat.2010.09.018 (2011).
529 35 Hirsch, P. B., Howie, A., Nicholson, R. B., Pashley, D. W. & Whelan, M. J.
530 *Electron Microscopy of Thin Crystals*. (Butterworths, London, 1965).
531 36 Jenkins, M. L. & Kirk, M. A. *Characterization of Radiation Damage by
532 Transmission Electron Microscopy*. (Institute of Physics, Bristol and
533 Philadelphia, 2001).
534 37 Kiritani, M. Electron Radiation Induced Diffusion of Point Defects in Metals.
535 *Journal of the Physical Society of Japan* **40**, 1035-1042,
536 doi:10.1143/JPSJ.40.1035 (1976).
537 38 Nguyen-Manh, D., Horsfield, A. P. & Dudarev, S. L. Self-interstitial atom
538 defects in bcc transition metals: Group-specific trends. *Physical Review B* **73**,
539 020101 (R) (2006).
540 39 Oen, O. S. Cross sections for atomic displacements in solids by fast electrons.
541 (1965).
542 40 Hänggi, P., Talkner, P. & Borkovec, M. Reaction-rate theory: fifty years after
543 Kramers. *Reviews of Modern Physics* **62**, 251-341 (1990).
544 41 Dudarev, S. L. Coherent motion of interstitial defects in a crystalline material.
545 *Philos Mag* **83**, 3577-3597, doi:10.1080/14786430310001599388 (2003).
546 42 Benderskii, V., Makarov, D. & Wight, C. *Chemical Dynamics at Low
547 Temperature*. (Wiley-Interscience, 1994).
548 43 Wang, C. Z., Chan, C. T. & Ho, K. M. Tight-binding molecular-dynamics
549 study of phonon anharmonic effects in silicon and diamond. *Physical Review
550 B* **42**, 11276-11283 (1990).

551

Figures

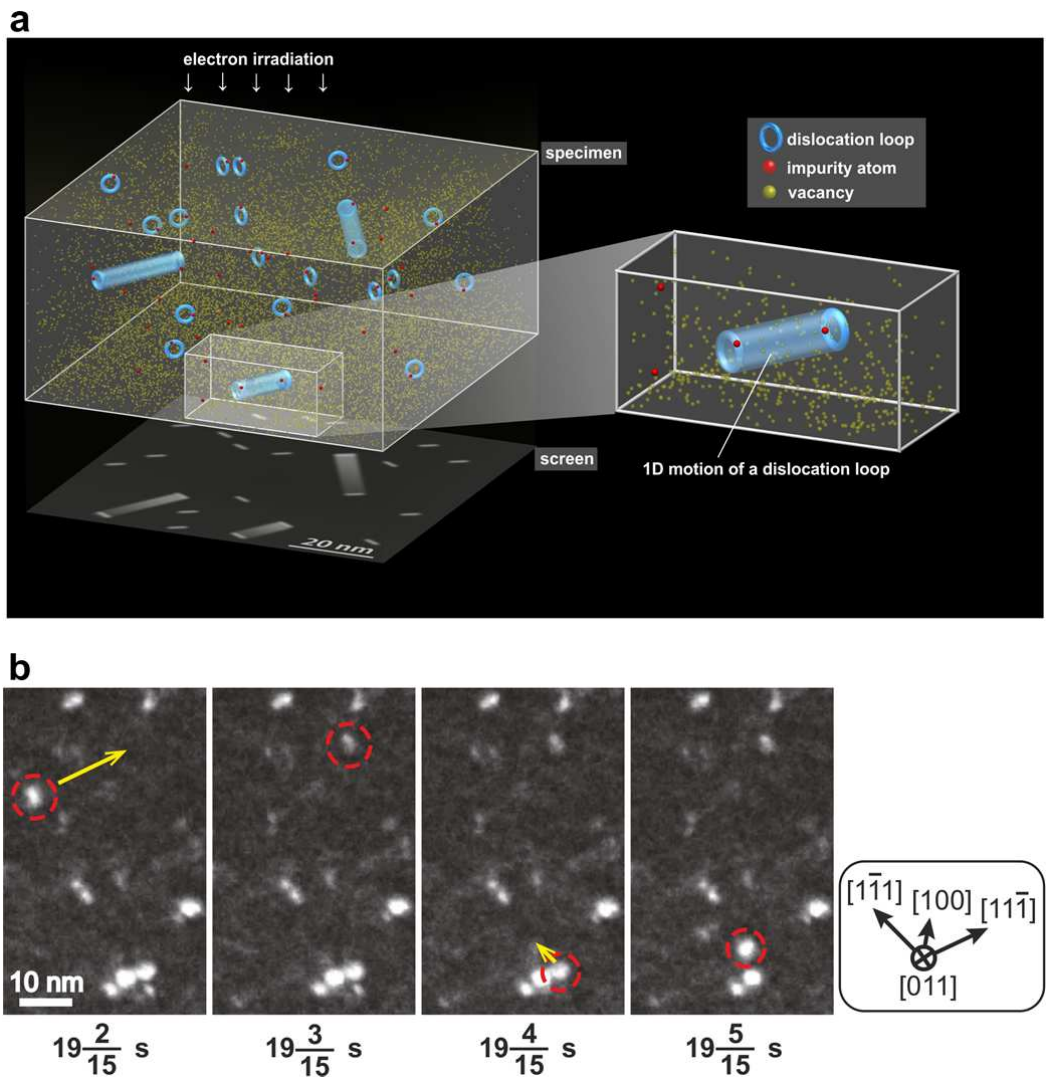

Figure 1 | 1D SIA cluster motion. a, Experimental setup. In a high-purity tungsten specimen, SIA clusters in the form of nanoscale ½<111> dislocation loops are trapped by impurity atoms at their boundary. **b,** High-energy electron irradiation enables clusters to escape, and subsequently undergo fast 1D glide diffusion before being trapped by other impurity atoms. This 1D motion was monitored simultaneously (acceleration voltage: 1000 kV; beam intensity: 2×10^{25} $m^{-2}s^{-1}$; temperature: 260 K, see Supplementary Video 1). Circled clusters move in the directions indicated by arrows, parallel to the <111>-type cluster Burgers vectors. The clusters hop distances of several nm to a few tens of nm within a single 1/15 s movie frame.

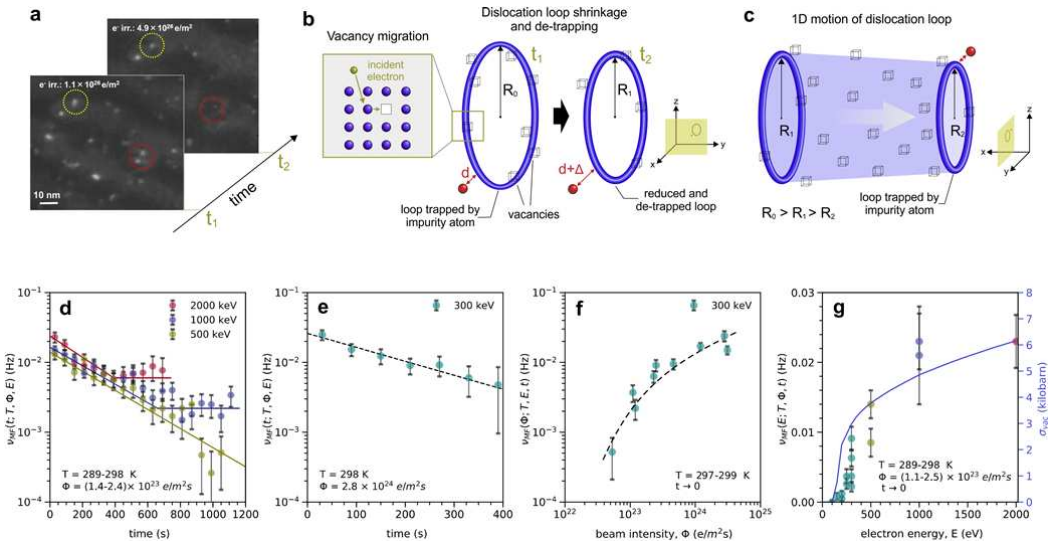

564

565 **Figure 2 | Characterization of the motion frequency of SIA cluster de-trapping. a,**
566 SIA cluster (dislocation loop) shrinking under the beam (acceleration voltage: 300
567 kV; beam intensity: 3.1×10^{24} $m^{-2}s^{-1}$; temperature: 299 K). Vacancies in tungsten are
568 thermally immobile at 299 K, and so the only way the SIA clusters can shrink is via
569 the absorption of radiation-mobilized vacancies. **b,** The clusters escape by increasing
570 the distance between their perimeter and the impurity, from d to $d + \Delta$, as they shrink
571 from radius R_0at time $t_1 \rightarrow R_1 < R_0$ at time t_2. This reduces the binding energy (see
572 Supplementary Discussion 1) **c,** Stop-and-go motion of the loop in the clouds of
573 vacancies and impurities. Once the loop has escaped from the impurity, it migrates
574 until is trapped by another impurity. During this macro-jump, over many Peierls
575 barriers, the loop sweeps through the surrounding vacancy clouds, decreasing its
576 effective radius to $R_2 < R_1$. **d, e,** Motion frequency decaying exponentially with time
577 under irradiation which corresponds to indirect mechanism (see Methods). Plateaus
578 are reached when the supply of vacancies local to the clusters is exhausted by
579 annihilation, and the direct mechanism takes over (see Methods). **f,** Motion frequency
580 increasing with beam intensity (time: 0 – 60 s). **g,** Motion frequency vs. beam energy
581 and cross section for radiation-induced vacancy migration (time: 0 – 60 s) (see
582 Methods).

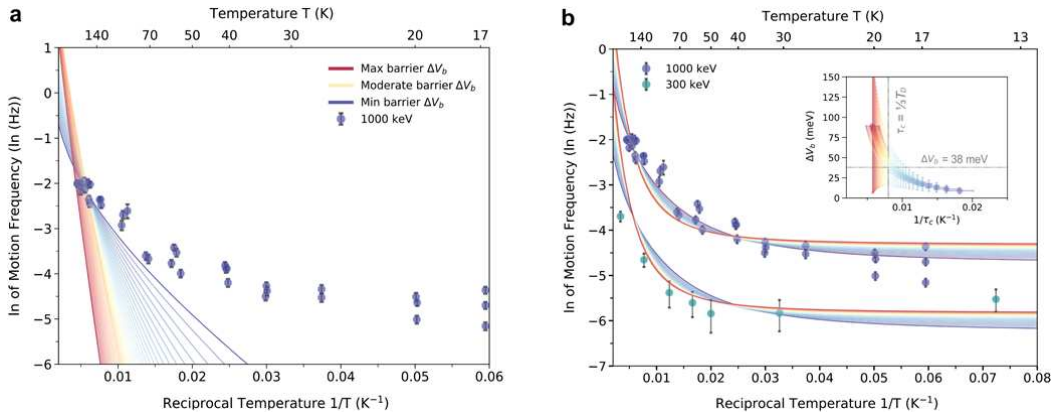

583

584 **Figure 3** | **Motion frequency of SIA cluster de-trapping vs. temperature.** Data
585 points show measured motion frequency vs. temperature (data taken in first 60 s of
586 irradiation. Blue points: beam energy 1000 keV, beam intensity 2×10^{25} $m^{-2}s^{-1}$; green
587 points: beam energy 300 keV, beam intensity $(2-4) \times 10^{24}$ $m^{-2}s^{-1}$). Some error bars
588 are too small to be visible. **a,** All possible classical fits of one single dataset, at beam
589 energy of 1000 keV, for activation barriers between 10 meV (blue) and 90 meV (red).
590 Thin lines between are intermediate values. No classical fit can capture the
591 temperature dependence. **b,** As panel a but using quantum mechanical rate function.
592 Both 1000 and 300 keV datasets were fitted simultaneously, with a single parameter
593 to account for the ratio of the two (we obtained a value of 4.52 for the ratio, consistent
594 with Fig. 2g, see Methods). Inset: fitted correlation between activation barrier and
595 critical temperature τ_c (see text and Methods), with corresponding error bars. The
596 value of the effective activation barrier at $\tau_c = \frac{1}{3}T_D$ (T_D: Debye temperature) is 38
597 meV.

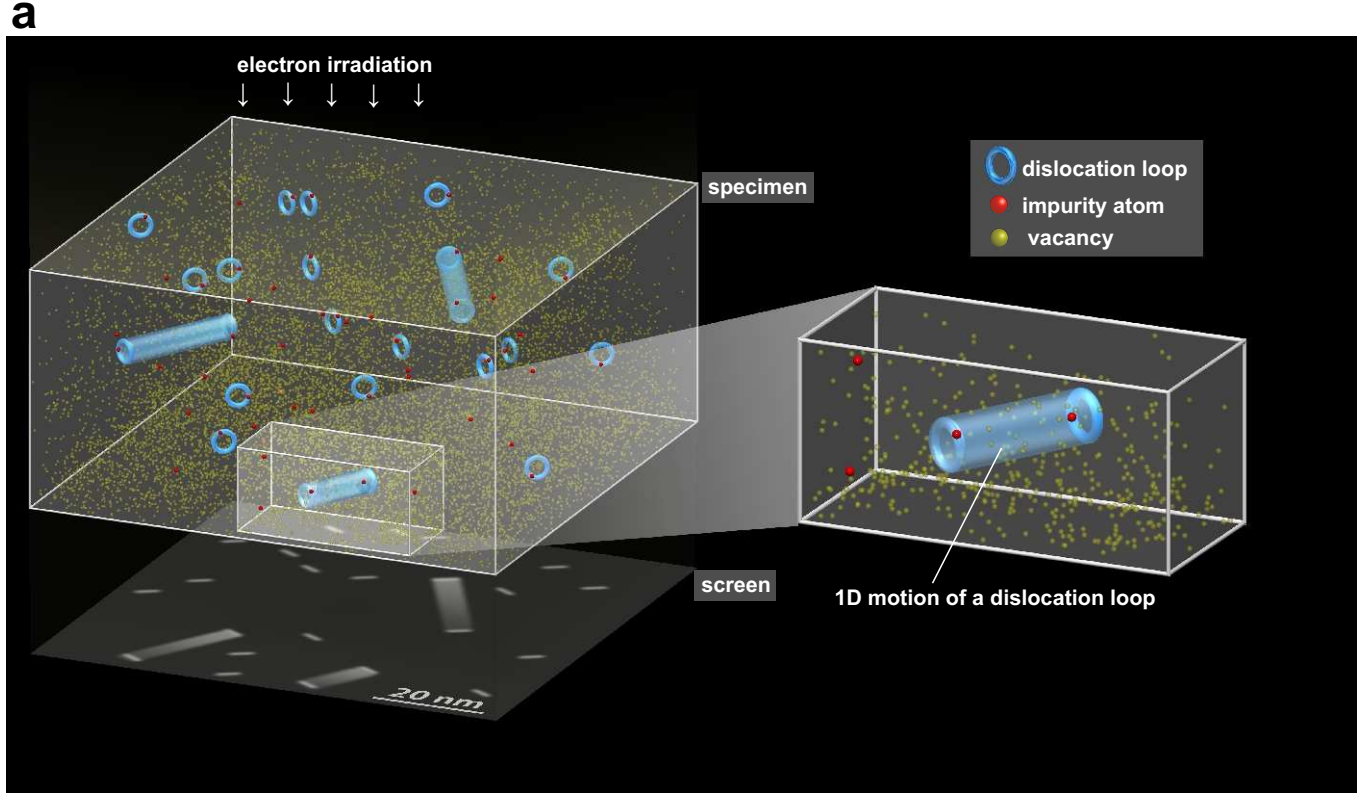
a
electron irradiation
specimen
dislocation loop
impurity atom
vacancy
screen
1D motion of a dislocation loop
20 nm

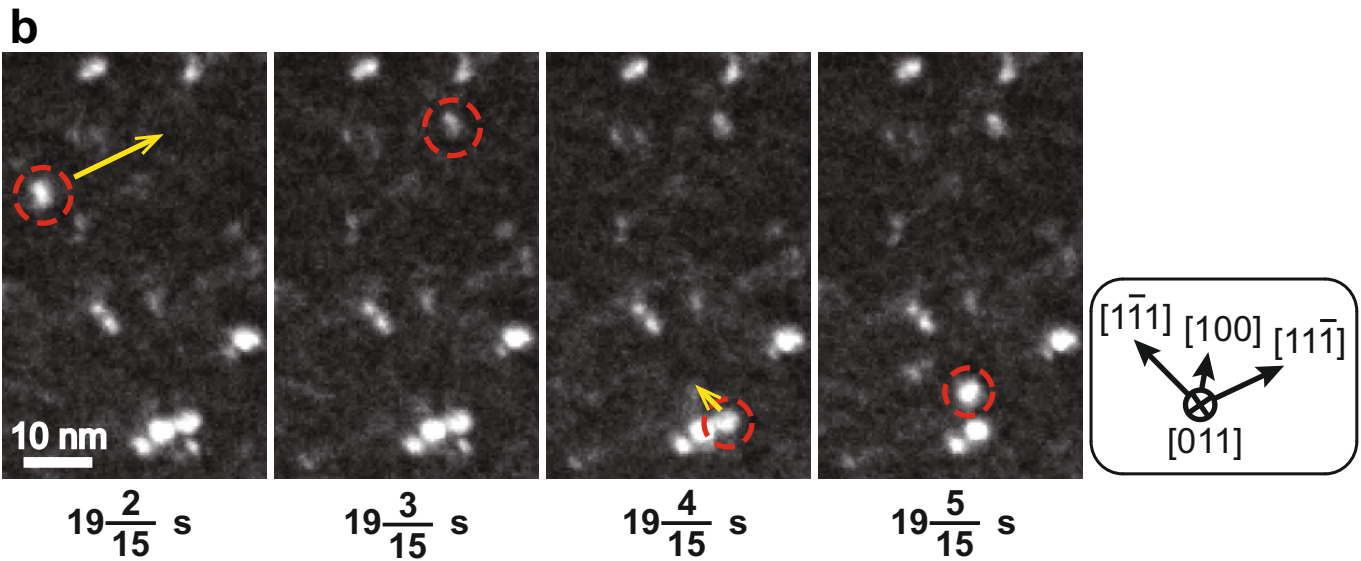
b
10 nm
$19\frac{2}{15}$ s
$19\frac{3}{15}$ s
$19\frac{4}{15}$ s
$19\frac{5}{15}$ s
[1$\bar{1}$1]
[100]
[11$\bar{1}$]
[011]

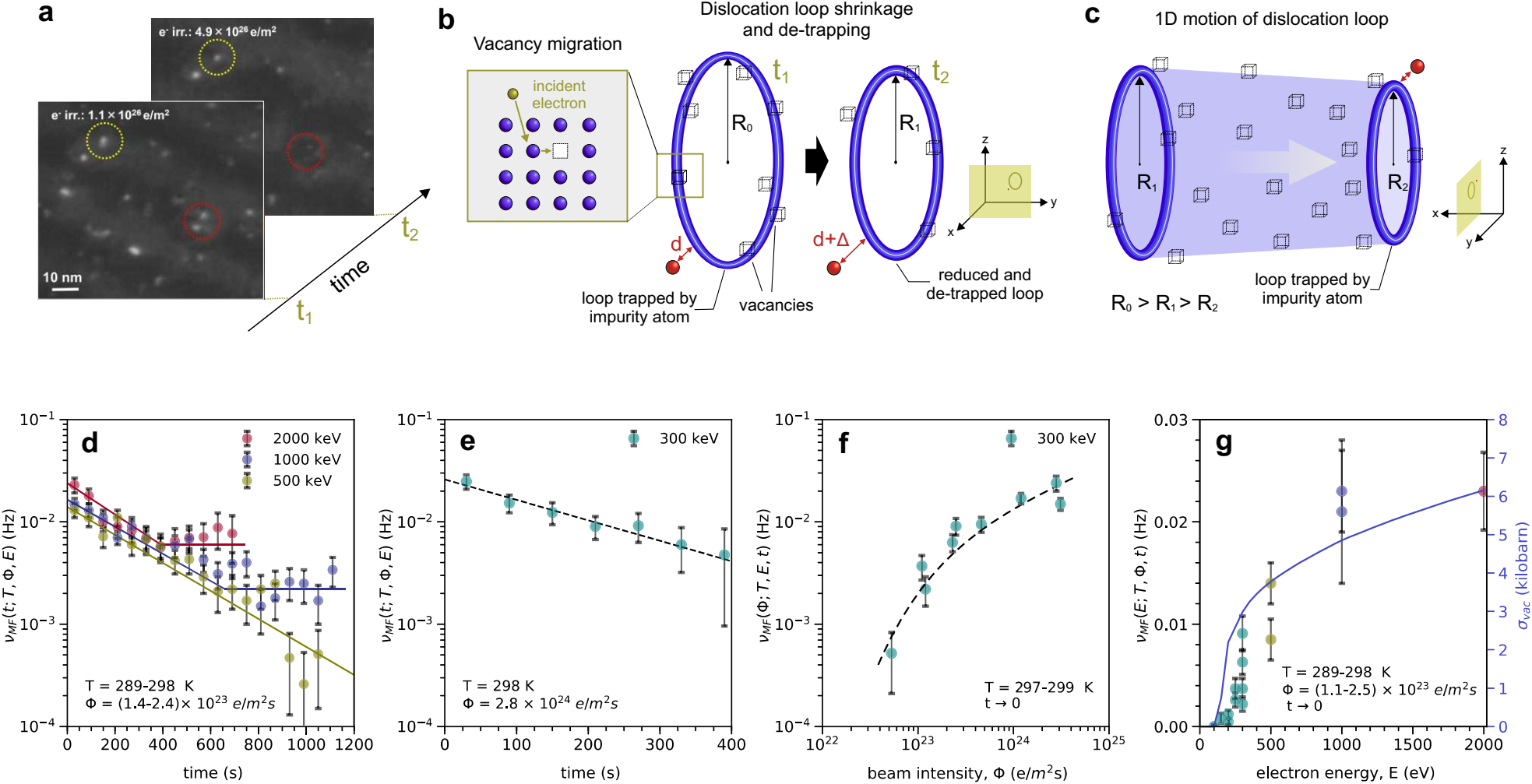
a
e⁻ irr.: 4.9 × 10²⁶ e/m²
e⁻ irr.: 1.1 × 10²⁶ e/m²
10 nm
t₂
time
t₁
b
Vacancy migration
Dislocation loop shrinkage and de-trapping
incident electron
t₁
R₀
d
t₂
R₁
d+Δ
z
y
x
loop trapped by impurity atom
vacancies
reduced and de-trapped loop
c
1D motion of dislocation loop
R₁
R₂
z
x
y
R₀ > R₁ > R₂
loop trapped by impurity atom
d
2000 keV
1000 keV
500 keV
T = 289-298 K
Φ = (1.4-2.4)× 10²³ e/m²s
time (s)
e
300 keV
T = 298 K
Φ = 2.8 × 10²⁴ e/m²s
time (s)
f
300 keV
T = 297-299 K
t → 0
beam intensity, Φ (e/m²s)
g
T = 289-298 K
Φ = (1.1-2.5) × 10²³ e/m²s
t → 0
electron energy, E (eV)
σvac (kilobarn)

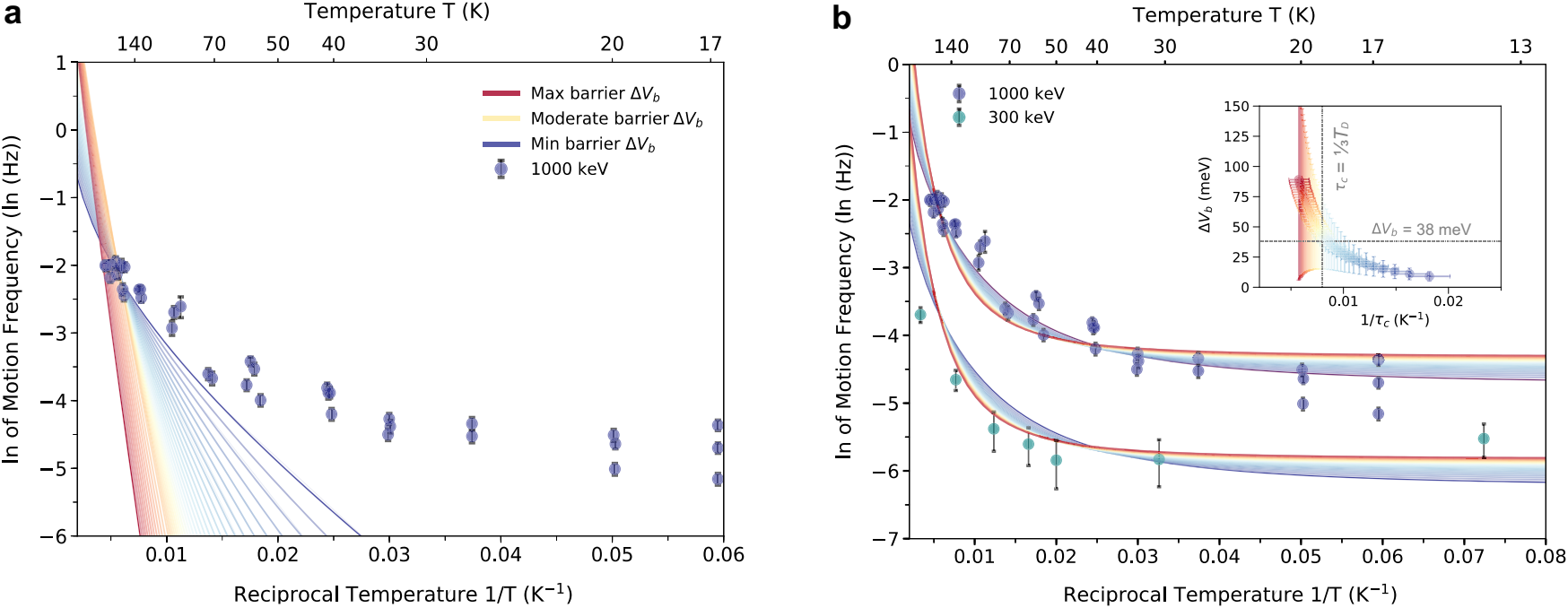
a
Temperature T (K)
140
70
50
40
30
20
17
Max barrier ΔV_b
Moderate barrier ΔV_b
Min barrier ΔV_b
1000 keV
ln of Motion Frequency (ln (Hz))
Reciprocal Temperature 1/T (K^{-1})
b
Temperature T (K)
140
70
50
40
30
20
17
13
1000 keV
300 keV
ΔV_b (meV)
$\tau_c = 1/3T_D$
ΔV_b = 38 meV
$1/\tau_c$ (K^{-1})
ln of Motion Frequency (ln (Hz))
Reciprocal Temperature 1/T (K^{-1})

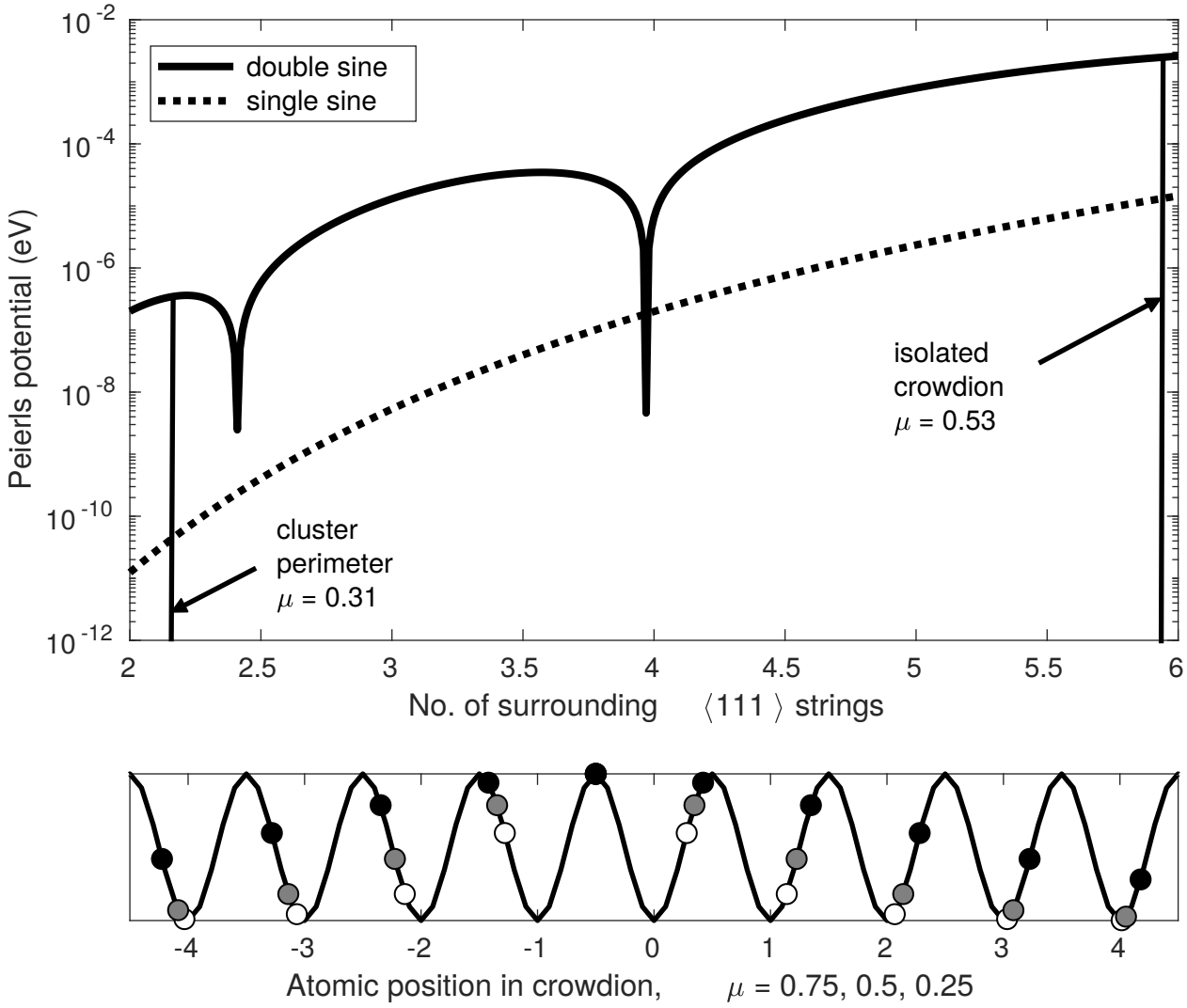
double sine
single sine
Peierls potential (eV)
10 -2
10 -4
10 -6
10 -8
10 -10
10 -12
isolated
crowdion
μ = 0.53
cluster
perimeter
μ = 0.31
2
2.5
3
3.5
4
4.5
5
5.5
6
No. of surrounding ⟨111⟩ strings
-4
-3
-2
-1
0
1
2
3
4
Atomic position in crowdion, μ = 0.75, 0.5, 0.25

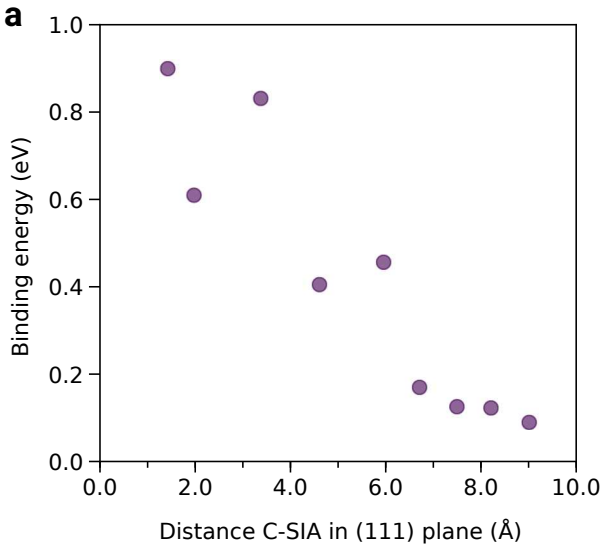
a
Binding energy (eV)
Distance C-SIA in (111) plane (Å)

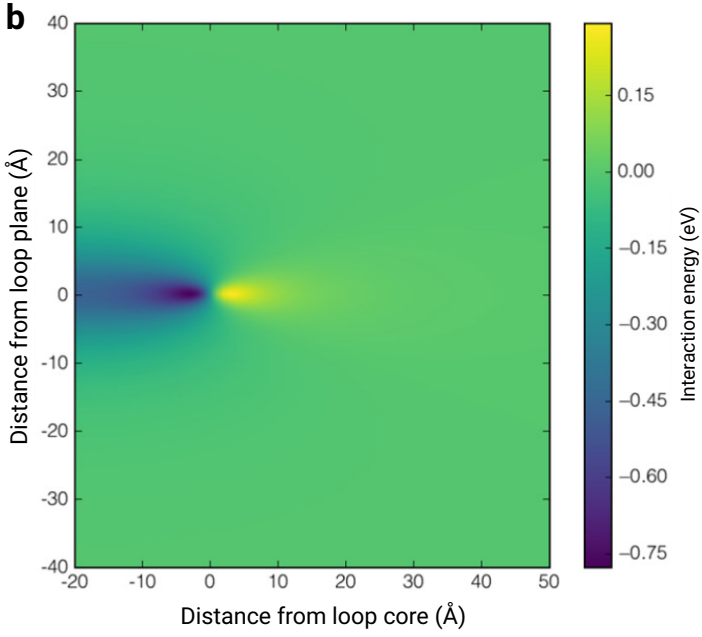
b
Distance from loop plane (Å)
Distance from loop core (Å)
Interaction energy (eV)

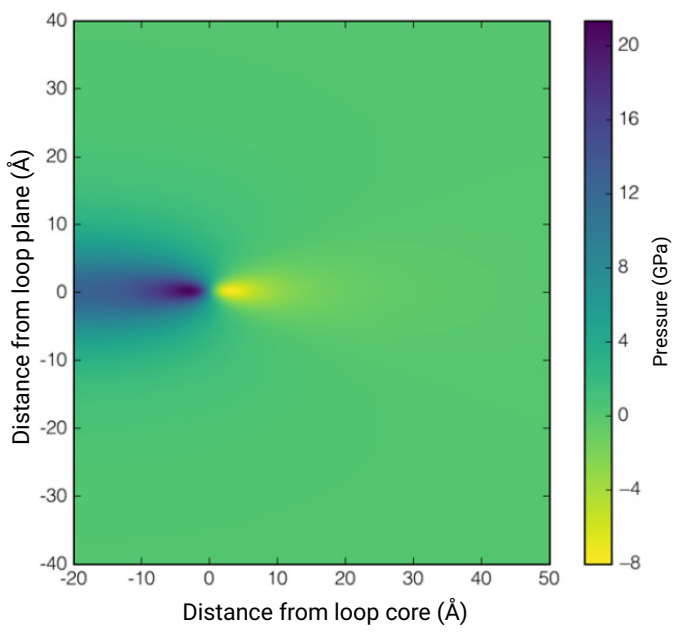
Distance from loop plane (Å)
Distance from loop core (Å)
Pressure (GPa)

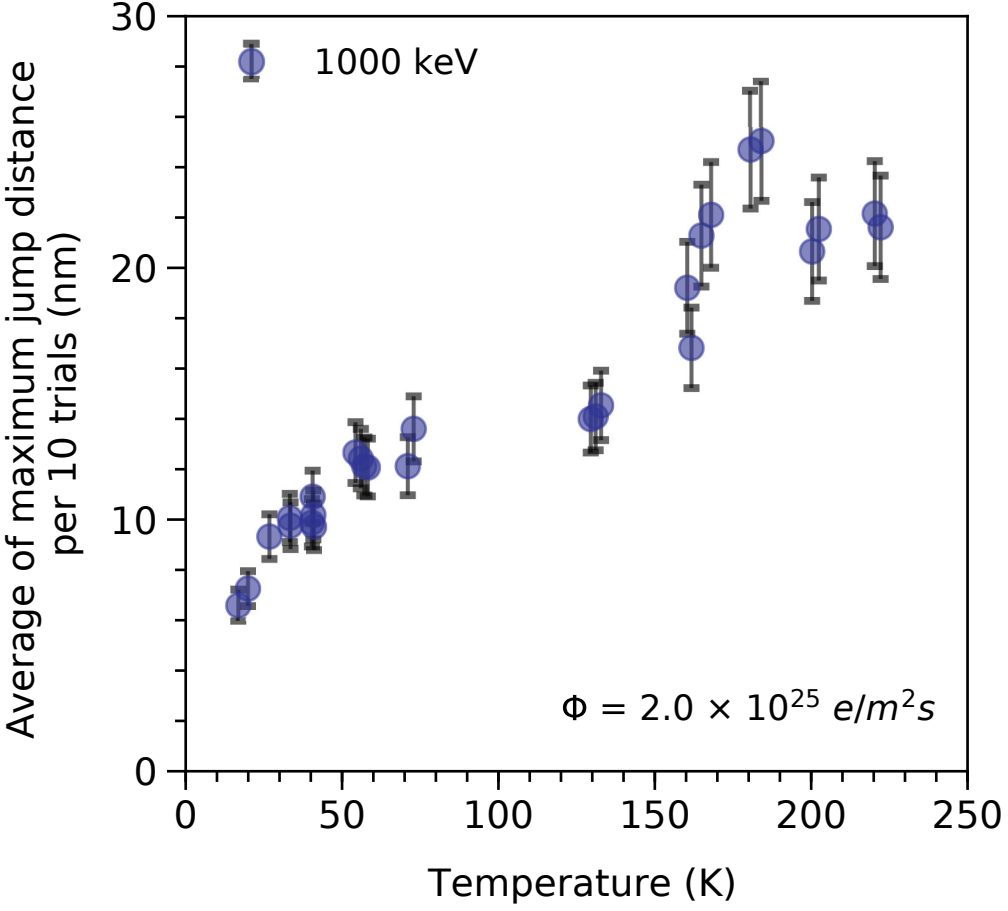
1000 keV
Φ = 2.0 × 10^25 e/m^2s
Average of maximum jump distance per 10 trials (nm)
Temperature (K)
0
10
20
30
0
50
100
150
200
250

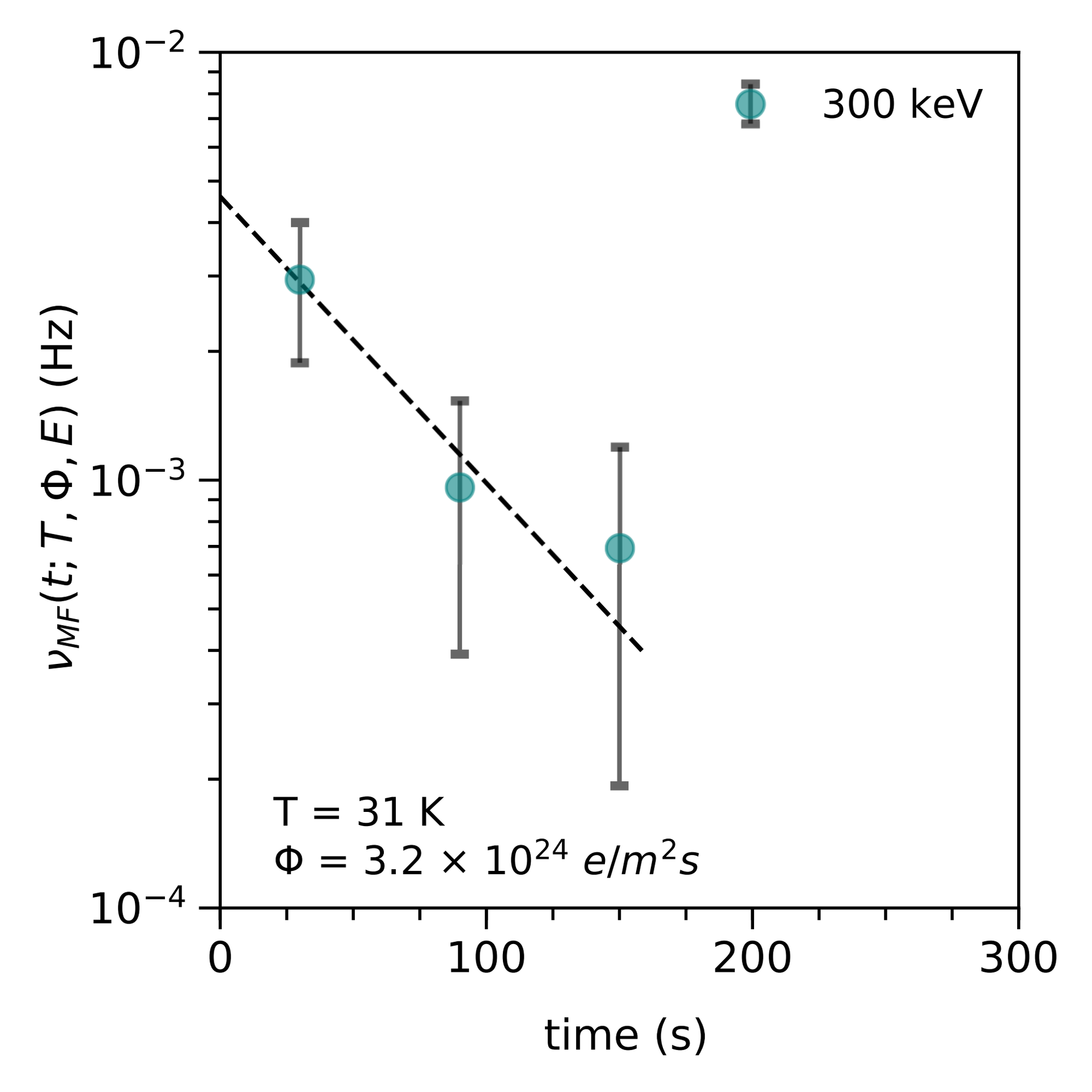
10^{-2}
10^{-3}
10^{-4}
$\nu_{MF}(t; T, \Phi, E)$ (Hz)
300 keV
T = 31 K
$\Phi = 3.2 \times 10^{24}\ e/m^2 s$
0
100
200
300
time (s)

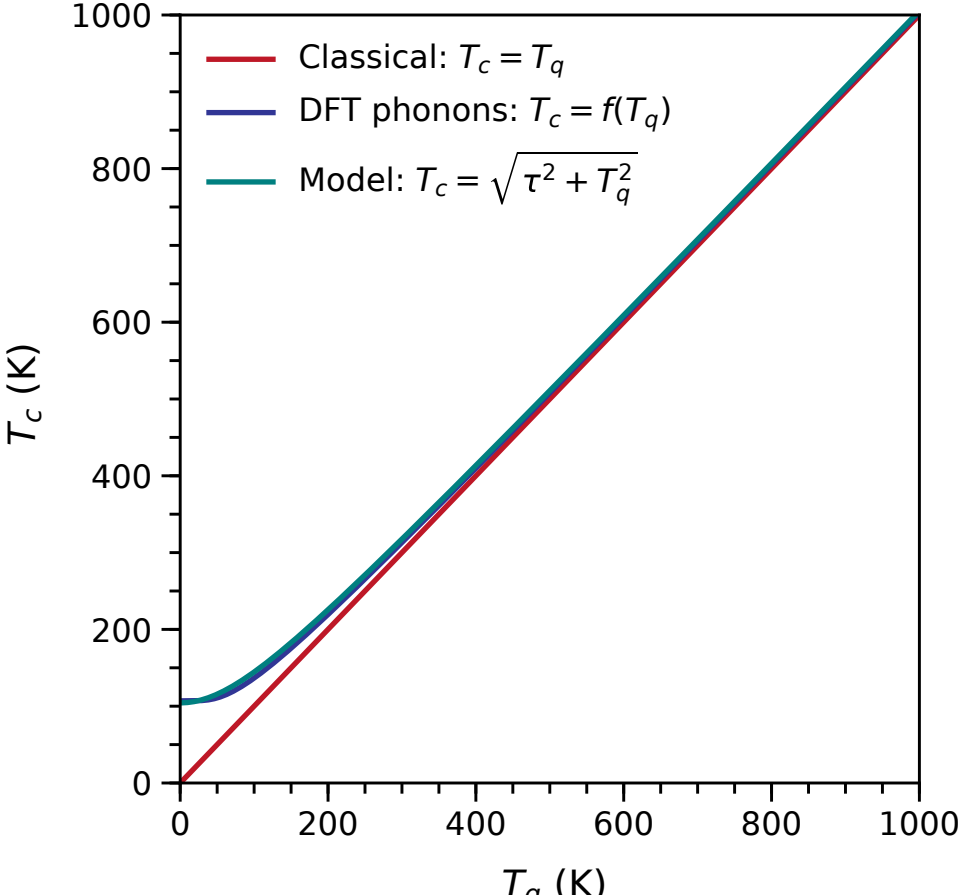
Classical: $T_c = T_q$
DFT phonons: $T_c = f(T_q)$
Model: $T_c = \sqrt{\tau^2 + T_q^2}$
T_c (K)
T_q (K)
0
200
400
600
800
1000

SUPPLEMENTARY INFORMATION

Quantum de-trapping and transport of heavy defects in tungsten

Kazuto Arakawa[1*], Mihai-Cosmin Marinica[2], Steven Fitzgerald[3], Laurent Proville[2], Duc Nguyen-Manh[4], Sergei L. Dudarev[4], Pui-Wai Ma[4], Thomas D. Swinburne[5], Alexandra M. Goryaeva[2], Tetsuya Yamada[6], Takafumi Amino[7], Shigeo Arai[8], Yuta Yamamoto[8], Kimitaka Higuchi[8], Nobuo Tanaka[8], Hidehiro Yasuda[9], Tetsuya Yasuda[9], Hirotaro Mori[9]

[1] *Next Generation TATARA Co-Creation Centre, Organization for Industrial Innovation, Shimane University, 1060 Nishikawatsu, Matsue 690-8504, Japan.*

[2]*DEN-Service de Recherches de Métallurgie Physique, CEA, Université Paris-Saclay, F-91191, Gif-sur-Yvette, France.*

[3]*Department of Applied Mathematics, University of Leeds, Leeds LS2 9JT, UK*

[4]*CCFE, United Kingdom Atomic Energy Authority, Culham Science Centre, Oxfordshire OX14 3DB, United Kingdom.*

[5]*CINaM-Aix Marseille Université-CNRS, 13009 Marseille, France.*

[6]*Railway, Automotive & Machinery Parts Unit Osaka Steel Works, Nippon Steel & Sumitomo Metal Corporation, 1-109, Shimaya 5-chome, Konohana-ku, Osaka 554-0024, Japan.*

[7]*Advanced Technology Research Laboratories, Nippon Steel & Sumitomo Metal Corporation, 1-8 Fuso-Cho, Amagasaki, Hyogo 660-0891, Japan.*

[8]*Institute of Materials and Systems for Sustainability, Nagoya University, Nagoya 464-8603, Japan.*

[9]*Research Centre for Ultra-High Voltage Electron Microscopy, Osaka University, 7-1 Mihogaoka, Ibaraki, Osaka 567-0047, Japan.*

*email: arakawa@riko.shimane-u.ac.jp

Supplementary Discussion

Supplementary Discussion 1 | Energetics of SIA cluster escape and migration

1a. Suppression of the cluster Peierls potential

The one-dimensional nature of the crowdion defect means the analytically tractable Frenkel-Kontorova (FK) model[1] can be applied, which yields the following expression for the static displacement field u as a function of the distance along the ⟨111⟩ string, x:

$$u(x) = \frac{2}{\pi}\tan^{-1}\exp\big(\mu(x - x_0)\big),$$

in units where the atomic spacing along the ⟨111⟩ string (0.274nm), is set equal to 1, and x_0 is the location of the defect's centre. $u \to 0$, 1 as $x \to \mp\infty$ reflecting the additional atom inserted in the string. $\mu < 1$ is a parameter measuring the degree of delocalization: as μ decreases, the defect spreads out, and the number of atoms N involved increases ($N = 1/\mu = 1.9$ in tungsten[2]). This has profound consequences for the interaction of crowdions with the lattice and other defects. The *effective mass* of the defect (defined via the kinetic term in the effective Lagrangian[3,4]) scales with $\mu < 1$. The crowdion moves along the string through a potential due to the surrounding lattice (period a, known as the *Peierls* potential) proportional to $\mathrm{cosech}(\pi^2/\mu) \approx 2\exp(-\pi^2/\mu)$ [4,5] for the case of the single-sine model. A more complicated expression[5] results when the more accurate double-sine model is used, but the conclusion is unchanged. For $\mu < 1$ this corresponds to a strong suppression.

An isolated crowdion is surrounded by 6 undefected ⟨111⟩ strings, which act to compress the defect along its axis. A crowdion at the edge of a cluster, however, is surrounded by fewer undefected strings – 2 or 3 depending on the boundary configuration[3]. This reduces μ by a factor of $\sqrt{2}$ to $\sqrt{3}$, which corresponds to an enormous suppression of the Peierls potential, thanks to its extreme nonlinearity in μ, completely overwhelming the increased number of crowdions in a cluster that interact with the Peierls potential compared with an isolated crowdion. This explains why the clusters can move quasi-freely once they have escaped from the traps (see Fig. ED1).

1b. Cluster binding energies

The FK model can be extended to include impurities such as C and N, or vacancies,

by modifying the defect's coupling to one lattice site in the discrete FK model. This leads to the effective impurity interaction potential[6,7]: $V^I(x_0) = \mu\Delta \mathrm{sech}^2(\mu x_0)$, where Δ is proportional to the strength of the interaction, and can be determined from density functional studies; x_0 is the distance of the crowdion from the impurity/vacancy along the ⟨111⟩ string. The interaction is short-ranged, decreasing with the separation towards zero within a few lattice spacings (Fig. ED2a, see also Ref. [8]). For C, $\mu_1\Delta \approx 0.9$ eV[8], where μ_1 corresponds to a single isolated crowdion. Note that the delocalization parameter μ affects both the depth and the breadth of the impurity potential well.

Transverse to the ⟨111⟩ direction, the interaction can be well modelled by elasticity, treating the impurity as a dilatation centre that couples to the hydrostatic part of the cluster's stress field. Fig. ED2b shows the binding energy closely following the hydrostatic pressure field of the cluster. In this approximation, the corresponding energy landscape for any impurity is the same, merely scaled by the $\mu\Delta$ value.

Supplementary Discussion 2 | Temperature

Now we turn to the local heating of the used specimen. Electron irradiation can locally heat the specimen via inelastic scattering[9], and to rule out this effect another quantity was monitored from the same movies: the distance that an escaped cluster travels before being trapped by another impurity atom. Figure ED3 shows the average of the maximum hop distance per 10 hops as a function of measured temperature. The impurity traps can be 5-20 nm apart. We measured the jumping distance with respect to the irradiation time (at a given temperature, the jumping distance is not dependent on the irradiation time). The key point is that there is a range of barriers, depending on the separation of each impurity from the cluster's glide cylinder, which vary over almost an order of magnitude. These appear in the exponent of the rate, so have a significant effect. In the high temperature limit, the loops can escape from high trapping energies, i.e., the loops are trapped only by the impurities that are in the close neighbourhood of the loop (small loop-impurity separation gives high trapping energy). At lower temperatures, the loops can only escape from lower trapping energies, i.e. in this regime, the loops can be trapped by more distant impurities. So, at lower temperatures, more of the impurities distributed through the sample will contribute to the trapping, whilst at higher temperatures, fewer will. This means that

the jumping distance will decrease with temperature. The recorded data confirm this, and we conclude that the local temperature at the irradiated continues to decrease down to the lowest measured values.

References

1 Braun, O. M. & Kivshar, Y. *The Frenkel-Kontorova model: concenpts, methods, and applications*. (Springer Science & Business Media, 2013).

2 Derlet, P. M., Nguyen-Manh, D. & Dudarev, S. L. Multiscale modeling of crowdion and vacancy defects in body-centered-cubic transition metals. *Physical Review B* **76**, 054107 (2007).

3 Dudarev, S. L. Coherent motion of interstitial defects in a crystalline material. *Philos Mag* **83**, 3577-3597, doi:10.1080/14786430310001599388 (2003).

4 Kosevich, A. M. *The Crystal Lattice: Phonons, Solitons, Dislocations, Superlattices*. (Wiley, 2006).

5 Fitzgerald, S. P. & Nguyen-Manh, D. Peierls potential for crowdions in the bcc transition metals. *Physical Review Letters* **101**, 115504 (2008).

6 Braun, O. M. & Kivshar, Y. S. Nonlinear dynamics of the Frenkel-Kontorova model with impurities. *Physical Review B* **43**, 1060-1073 (1991).

7 Fitzgerald, S. P. Crowdion–solute interactions: Analytical modelling and stochastic simulation. *Nuclear Instruments and Methods in Physics Research Section B: Beam Interactions with Materials and Atoms* **352**, 14-17, doi:http://dx.doi.org/10.1016/j.nimb.2014.10.003 (2015).

8 Kong, X.-S. *et al.* First principles study of foreign interstitial atom (carbon, nitrogen) interactions with intrinsic defects in tungsten. *J Nucl Mater* **430**, 270-278, doi:http://dx.doi.org/10.1016/j.jnucmat.2012.07.008 (2012).

9 Fisher, S. B. On the temperature rise in electron irradiated foils. *Radiation Effects* **5**, 239-243, doi:10.1080/00337577008235027 (1970).